AIAA JOURNAL
Vol. 45, No. 8, August 2007

Linear Stability Properties of Lifting Vortices over Delta Wings

Florent Renac* and Laurent Jacquin†
ONERA, 92230 Chatillon, France

DOI: 10.2514/1.25827

The purpose of this study is to apply existing theories of linear temporal instability and critical-state concept on realistic delta wing flows. Three-dimensional laser Doppler velocimetry measurements are performed on two delta wings with different geometries in transverse planes both upstream and downstream of the vortex breakdown. Representative models of the velocity fields in the leading-edge vortices are deduced from these measurements and allow us to examine the stability properties of such flows. As expected, helical modes are destabilized downstream of the breakdown with characteristics that agree with generalized centrifugal instability theory for large azimuthal wave numbers. Upstream of the breakdown, the perturbations are stabilized or weakly amplified. Moreover, a simple criticality criterion is shown to efficiently describe the conditions of breakdown in our experiments. These results suggest that inviscid and linear stability analysis based on the mean velocity field is sufficient to account for the linear stability behavior of delta wing flows at high Reynolds numbers.

Nomenclature

c	=	root chord length
c_-	=	minimum phase velocity
q, q_0	=	swirl numbers
Re_c, Re	=	Reynolds numbers
U, V, W	=	velocity components in the X, Y, and Z directions
U_x, V_r, W_θ	=	velocity components in the x, r, and θ directions
U_0	=	freestream velocity
u	=	external flow parameter
X, Y, Z	=	Cartesian frame
x, r, θ	=	cylindrical frame
α	=	angle of attack
φ	=	sweep angle
Ω_X, Ω_Z	=	vorticity components in the X and Z directions
Ω_x, Ω_θ	=	vorticity components in the x and θ directions
Ω_0	=	rotation rate of the vortex on its axis

I. Introduction

DELTA wing flows have been thoroughly investigated for both their fundamental and applicational interests. From a fundamental point of view, the delta wing is an efficient system to produce an intense and coherent vortical flowfield. It is also of great interest for aerodynamic and engineering issues because it constitutes a simple model of some military aircraft shapes. When the delta wing is set at incidence, the flow separation from the leading edge provides a shear layer. After rolling up, a vortex core develops and strong swirl is produced [1]. The resulting vortex, known as either a leading-edge vortex or primary vortex, is considered to be an important source of lift. It has a dominant effect on the delta wing flow properties. The strength of the primary vortex increases with the angle of incidence of the wing until the structure undergoes a brutal disorganization, the so-called vortex breakdown. This phenomenon leads to a deterioration of the lift characteristics and flow stationarity and leads to poor wing controllability. The vortex breakdown occurrence and related mechanisms are still not well understood despite numerous experimental, theoretical, or numerical investigations (reviews on the subject are provided in [2,3]) and efficient control techniques have not yet been achieved [4].

In this paper, we analyze laser Doppler velocimetry (LDV) measurements acquired in the flowfield over a rounded leading-edge delta wing with a sweep angle of $\varphi = 60$ deg. We compare them with results obtained with a second delta wing with a different geometry, defined by a sharp leading edge and a $\varphi = 70$-deg sweep angle. Results on the former model flowfield are presented in [5], and the latter flowfield is described in [6]. The smaller sweep angle and the rounded leading edge make the former model more representative of a real military aircraft. With respect to the $\varphi = 70$-deg delta wing, the vortices are weaker and the separation line is not fixed by a geometrical singularity.

The main objective of this work is to evaluate the inviscid linear temporal stability properties of the leading-edge vortices over both wings. Using the experimental data, the paper addresses the two following questions:

1) Concerning the temporal instability, do the existing theories apply to delta wing flows?

2) What can we learn concerning breakdown from the local properties of the velocity field measured upstream and downstream of it?

For that purpose, we introduce a velocity model representative of the measurements that allows the description of the flowfield both upstream and downstream of the vortex breakdown location. We conduct the temporal stability analysis of such a model using both analytical criteria and a spectral collocation method. Then predictions are compared with the occurrence of vortex breakdown.

The hydrodynamic stability analysis of inviscid, incompressible, and permanent columnar vortices has been intensively theoretically and numerically explored by studying the evolution of normal modes superimposed on a basic flow. This concept assumes that the basic flow is laminar. This hypothesis holds upstream of the vortex breakdown, but is not verified downstream of it, where the flow supports a wide range of scales of motion. Studies of the interaction between large coherent structures and fine scales in turbulent shear flows underscore the stabilizing character of the turbulence on the instabilities [7]. Hence, a stability analysis in the breakdown wake will overestimate the growth rates of the perturbations. However, vortices remain laminar upstream of the breakdown. The strong rotation levels stabilize the perturbations by dispersing their energy [8]. This feature validates an inviscid stability analysis upstream of the breakdown, which allows a comparison between critical conditions in the vortex and breakdown occurrence.

Received 13 June 2006; revision received 1 May 2007; accepted for publication 1 May 2007.

*Research Engineer, Fundamental and Experimental Aerodynamics Department, 29 Avenue de la Division Leclerc.

†Head, Fundamental and Experimental Aerodynamics Department, 29 Avenue de la Division Leclerc. Member AIAA.

Destabilizing mechanisms could be present in a swirling jet, and the interest in vortex dynamics has led to the establishment of instability criteria. Lessen et al. [9] conducted linear temporal instability calculations for a q vortex [10] that represents wingtip vortices and swirling pipe flows. In the presence of azimuthal velocity, the negative helical modes are more destabilized than the corresponding positive modes. Increasing the swirl number q tends to amplify negative disturbances and to stabilize positive disturbances. The basic flow reaches stability for a sufficiently large swirl amount ($q > 1.5$). These results were later confirmed by the asymptotic analysis for great azimuthal wave numbers m of Leibovich and Stewartson [11] (hereafter referenced as LS), who identify a centrifugal instability characterized by the amplification of a negative modes family for limited values of q. Garg and Leibovich [12] used the numerical simulations of Lessen et al. [9] to describe LDV measurements in the flowfield of a vortex tube. Theoretical predictions using a velocity model to fit experimental results are in good agreement with prominent oscillations in the wake of the vortex breakdown and suggest that the measured frequencies correspond to the $m = -1$ helical mode. Moreover, Gursul [13] observed coherent surface pressure and velocity fluctuations, with a frequency corresponding to a $|m| = 1$ instability, in a delta wing flow downstream of the vortex breakdown. Similar coherent fluctuations were related either in the wake of a delta wing vortex breakdown [14] or in trailing vortices [15]. Likewise, unsteady small-scale vortices were observed in the shear layer that rolls up to form the primary vortex from numerical computations and were attributed to an inflectional mechanism [16]. Stability characteristics are, however, highly sensitive to the velocity model, and a detailed analysis with an accurate model is necessary to account for delta wing vortex dynamics.

Among theoretical vortex breakdown analyses, the critical-state concept advocated by Benjamin [17] focuses on neutrally stable inertial waves (or Kelvin waves) of infinite extent. According to Benjamin, vortex breakdown is the result of a transition from a supercritical flow supporting only downstream traveling waves to a subcritical flow supporting both upstream and downstream propagating waves. Experimental investigations of confined vortices in tubes [18,19] and direct numerical simulations of a free columnar vortex [20] confirm that vortex breakdown represents a transition from super- to subcritical flow, although the columnar flow assumption is violated around the vortex breakdown location. Nevertheless, the extension of these results to highly noncolumnar flows, such as delta wing flows, needs to be verified.

These aspects of the sensitivity of vortices to external linearized perturbations (helical modes behavior and the link between flow criticality and breakdown) will be analyzed using our data.

II. Experimental System and Technique

All experiments reported in this paper were conducted in the subsonic and atmospheric F2 wind tunnel at ONERA. The test section is rectangular with a width of 1.4 m, a height of 1.8 m, and a length of 5 m. Details of the facility are specified in [5]. In freestream conditions, turbulence level is approximately 0.1% of the mean velocity U_0 and the flow is uniform across the test section to within $\pm 1\%$. The delta wing is mounted on a sting, with a horizontal support for adjusting the angle of attack and for maintaining the wing close to the center axis of the test section.

In this study, we use two delta wing models with different geometrical characteristics. The first model possesses a rounded leading edge, a sweep angle of $\varphi = 60$ deg, and a root chord length of $c = 690$ mm (Fig. 1a). The second model has a sharp leading edge, a sweep angle of $\varphi = 70$ deg, and a chord length of $c = 950$ mm (Fig. 1b). In the following, model 1 and model 2 will refer to these models, respectively. Each model is beveled on the lower surface at an angle of 15 deg. The freestream incidences of model 1 ($\alpha = 18$ deg) and model 2 ($\alpha = 30$ deg) set the streamwise breakdown location X_b at about half of the root chord length (see Sec. III). The data are acquired for a freestream velocity $U_0 = 50$ m/s for model 1 and $U_0 = 24$ m/s for model 2. The freestream Reynolds numbers are $Re_c = U_0 c/\nu = 2.3 \times 10^6$ and 1.5×10^6, respectively. The projected frontal areas amount to 3.4 and 6.5% of the test section for models 1 and 2.

The three-dimensional LDV system uses two 15-W argon lasers as light sources in a forward-scattering mode. For each volume of exploration, the three instantaneous velocity components related to a specific particle are acquired. Incense smoke is used and allows Stokes numbers as low as $St < 5 \times 10^{-3}$, where $St = \tau_p/\tau_f$ relates the timescale of the particle $\tau_p = \rho_p d_p^2/18\mu$ ($\rho_p = 10^3$ kg/m^3 and $d_p = 0.5$ μm) to that of the flow. The flow timescale τ_f could be estimated either with the convection time $\tau_f = c/U_0$ or with the rotation rate of the vortex on its axis ($\tau_f = 2\pi/\Omega_0$). This allows neglecting particle lag bias due to inertia effects on our measurements. Moreover, precautions are taken to avoid virtual particle bias. Because of accessibility difficulties in the test section of the wind tunnel, an angle of 76.5 deg between laser beams is obtained, whereas a value of 90 deg is required to suppress such a

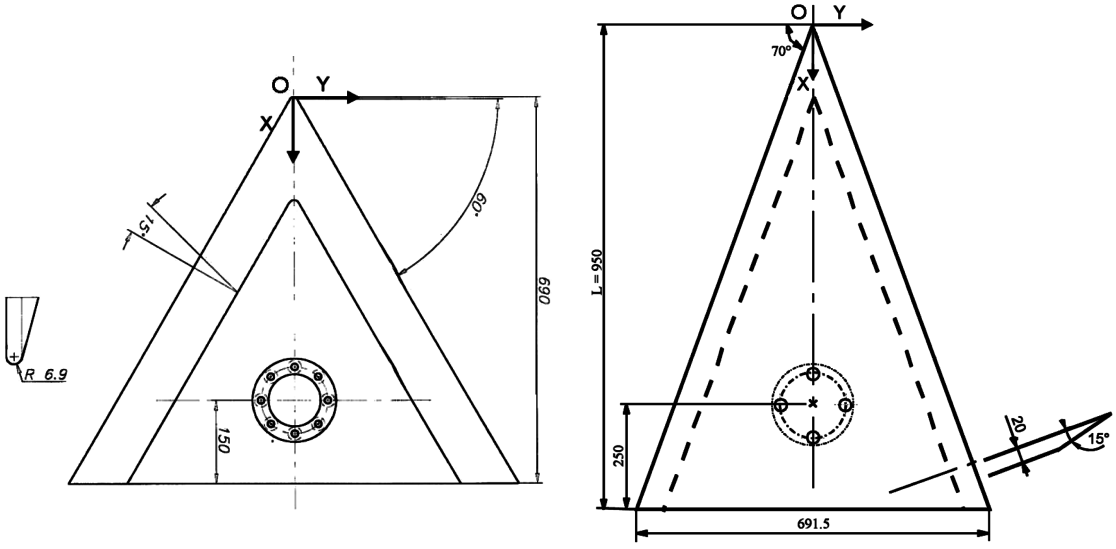

a) Model 1 b) Model 2

Fig. 1 Top view of both delta wing models with detail of the leading-edge shape and Cartesian coordinates X, Y, and Z; the Z axis is perpendicular to the leeward surface and dimensions are in millimeters.

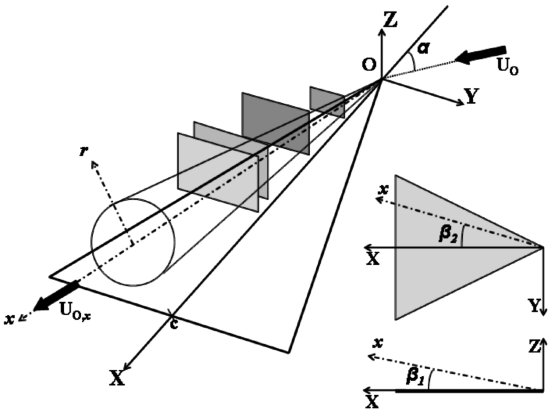

Fig. 2 Cartesian (X, Y, and Z) and cylindrical (x, r, and θ) coordinate systems and approximative measurement mesh positions.

bias. This value is, however, considered to be sufficient to neglect virtual particle bias [21].

The mean velocity components are calculated from samples of 2000 particles. Estimations of the uncertainties for each mean velocity and vorticity component are given in [5]. We retain global accuracies of $\sigma_U = 3\%$ and $\sigma_\Omega = 15\%$ for the velocity and vorticity components, respectively. These values are the sum of the natural variance of the flow and of uncertainties of the system and measurement techniques (processor resolution, fringe spacing, passage matrix coefficients, and Bragg frequency accuracies). The components of the velocity in the Cartesian frame (X, Y, and Z) attached to the delta wing model (Figs. 1 and 2) are denoted as U, V, and W, respectively.

The following results concern the port-side flowfield of each wing. The explored domain is composed of four transverse planes perpendicular to the root chord and one longitudinal plane intersecting the primary vortex axis and parallel to the wing surface. The spatial locations of the transverse planes are illustrated in Fig. 2. For model 1, the planes are located at $X/c = 0.22$, 0.36, 0.47, and 0.51 and consist of rectangular meshes containing approximately $N_p = 1200$ points evenly at intervals of $\Delta Y = \Delta Z = 1$ mm for the first plane and $\Delta Y = \Delta Z = 2$ mm for the other planes. The longitudinal plane extends from $X/c = 0.18$ to $X/c = 0.72$ and is constituted of $N_p = 535$ points. The mesh point spacing is $\Delta X = 25$ mm in the streamwise direction and $\Delta Y = 2$ mm in the spanwise direction. Planes are located at $X/c = 0.32$, 0.45, 0.53, and 0.84 over model 2. Each mesh is rectangular and uniform, with a spacing of $\Delta Y = \Delta Z = 5$ mm. $N_p = 165$, 441, 600, and 1183 points are used in the $X/c = 0.32$, 0.45, 0.53, and 0.84 planes, respectively. The longitudinal plane extends from $X/c = 0.32$ to 0.63 and is made up of 290 points evenly spaced at intervals of $\Delta X = 25$ mm in the streamwise direction and $\Delta Y = 5$ mm in the spanwise direction. For comparison, the vortex core diameter (defined by the spacing between the extrema of azimuthal velocity) in the flowfield over model 1 is about 11 mm in the first plane $X/c = 0.22$ and about 28 mm in the last plane $X/c = 0.51$ (it ranges from 9 to 55 mm in the model 2 vortex). For both delta wing flowfields, data consist of two planes upstream of the vortex breakdown and two planes downstream.

III. LDV Results

A. Mean Vortex Breakdown Position

The vortex breakdown position has been characterized by means of LDV measurements in longitudinal planes. Following Rockwell [22], its location may be conveniently defined as the locus at which the azimuthal vorticity changes sign on the vortex axis. Using cylindrical coordinates in a columnar flow, the azimuthal vorticity reads $\Omega_\theta = -\mathrm{d}U_x/\mathrm{d}r$, where U_x denotes the longitudinal velocity. Thus, the sign of azimuthal vorticity switches when the flow evolves from a jetlike to a wakelike type. Here, instead of Ω_θ, we use distributions of vertical vorticity $\Omega_Z = \partial V/\partial X - \partial U/\partial Y$ in the longitudinal plane intersecting the vortex core. The angle between the X and x axes fulfills $\beta_1 \ll 1$ (see Fig. 2), thus Ω_θ and Ω_Z components roughly match in an X–Y plane. The vorticity components are calculated from the mean velocity components measured in each plane and a first-order central-difference scheme. As already shown in [23], the switch of sign in vorticity patterns at the onset of breakdown results in a quadripolar structure with opposite signs of vorticity (Fig. 3). The vortex breakdown position is chosen as the center of this structure. Results indicate a mean vortex breakdown location at $X_b/c = 0.46 \pm 0.05$ over model 1 and $X_b/c = 0.50 \pm 0.05$ over model 2 (uncertainty of the mean vortex breakdown abscissa is defined by $\sigma_{X_b} = [1 + 4\sigma_\Omega^2/\Delta\Omega_Z^2]^{1/2}\Delta X/2$ and depends both on the mesh refinement ΔX and on the vorticity uncertainty σ_Ω; $\Delta\Omega_Z$ denotes the variation of vertical vorticity corresponding to the displacement ΔX). Note that downstream of the vortex breakdown, the region of positive azimuthal vorticity is surrounded by a region of negative vorticity (see Sec. IV.D).

B. Velocity and Vorticity Fields

Contours of nondimensional axial velocity U/U_0 in perpendicular planes are depicted in Fig. 4. Spanwise and crosswise coordinates are divided by the local half-span; that is, $Y/s = -1$ denotes the port-side leading edge. The classical structure of leading-edge vortices is recovered. Before breakdown (Figs. 4a and 4b), the flow has a jetlike profile characterized by a strong acceleration of the flow in the vortex core [1]. This acceleration is more pronounced in the model 2 flowfield, with values reaching $U/U_0 = 3.8$ on the axis, compared with $U/U_0 = 2.2$ over model 1. The presence of a jet results from the negative axial pressure gradient that is imposed by the increase in vortex circulation with distance from the apex [1]. Note that the flow keeps an axisymmetric distribution of velocity close to its centerline.

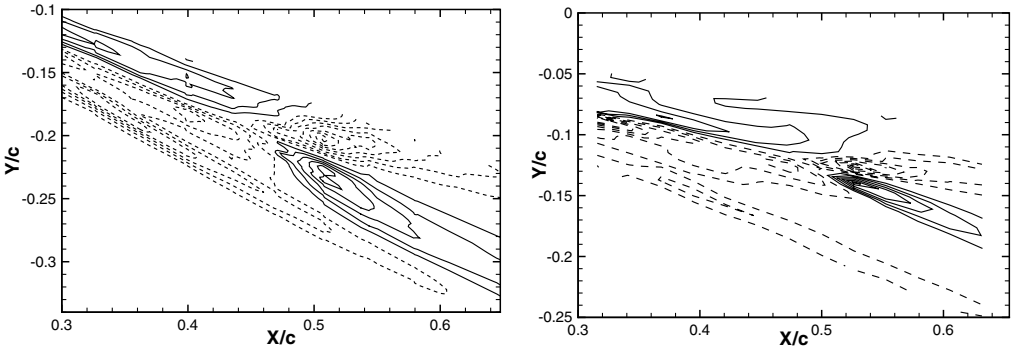

a) Model 1 **b) Model 2**

Fig. 3 Contours of nondimensional vertical vorticity $\Omega_Z c/U_0$ in the streamwise plane passing through the vortex core: a) model 1 and b) model 2; solid lines represent positive values and dashed lines represent negative values.

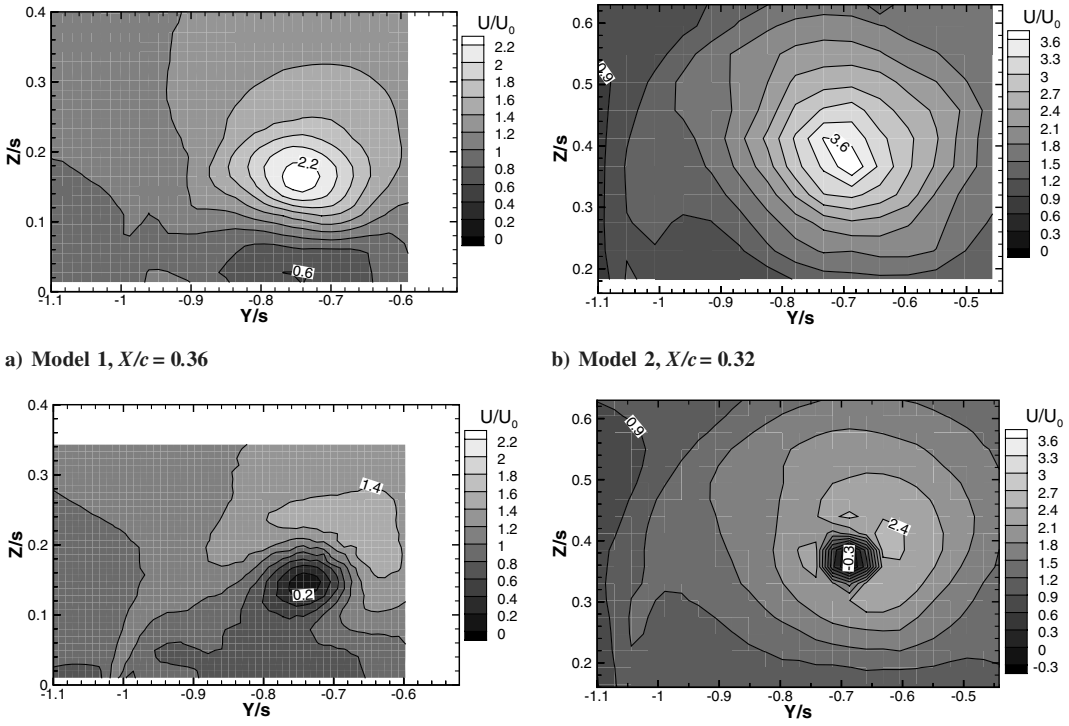

a) Model 1, $X/c = 0.36$ b) Model 2, $X/c = 0.32$

c) Model 1, $X/c = 0.51$ d) Model 2, $X/c = 0.53$

Fig. 4 Contours of U/U_0 in transverse planes upstream (top) and downstream (bottom) of the vortex breakdown location.

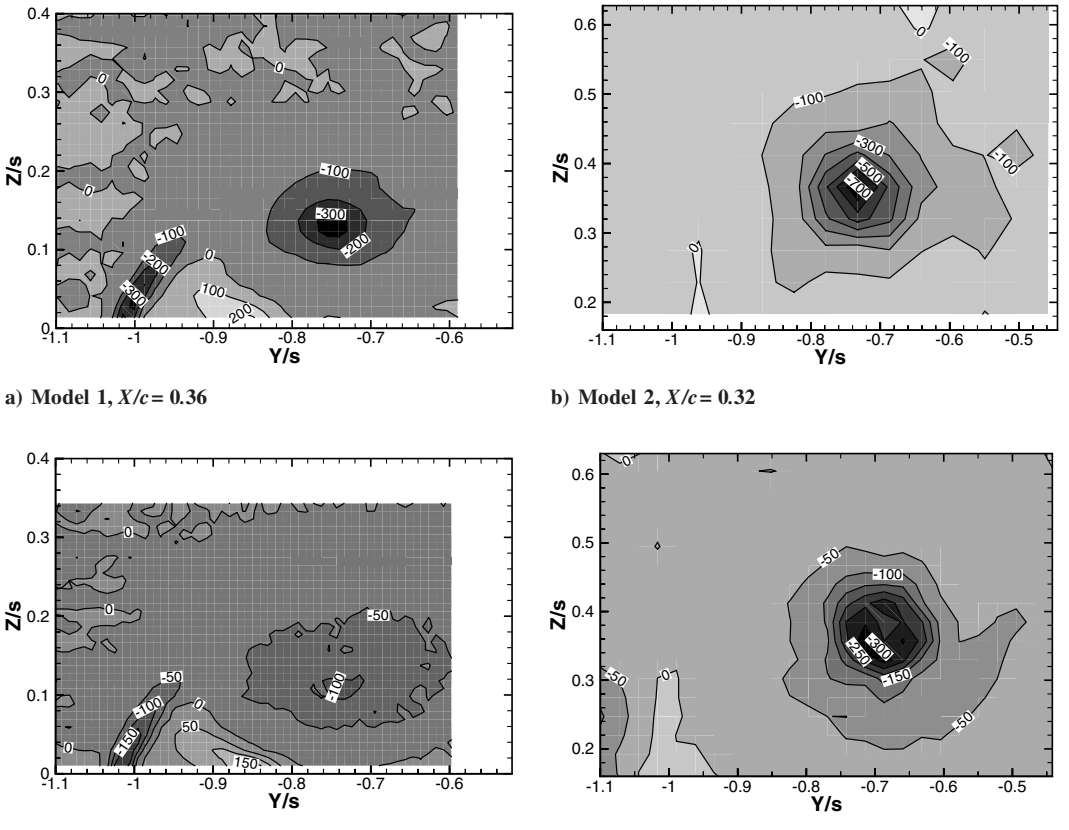

a) Model 1, $X/c = 0.36$ b) Model 2, $X/c = 0.32$

c) Model 1, $X/c = 0.51$ d) Model 2, $X/c = 0.53$

Fig. 5 Contours of $\Omega_X c/U_0$ in transverse planes upstream (top) and downstream (bottom) of the vortex breakdown location.

Farther from the axis, the wing and the shear layer, emanating from the leading edge, disrupt this symmetry (see Fig. 5). Downstream of the breakdown (Figs. 4c and 4d), the axial flow undergoes a strong decay [14]. The velocity distribution evolves to a wakelike profile due to the slowing down of the axial flow around the vortex centerline as a consequence of vortex breakdown [2,14]. The recirculation zone is absent in the breakdown wake over model 1, whereas axial flow reverses on the axis over model 2.

Figure 5 presents nondimensional axial vorticity isolevels $\Omega_X c/U_0$ in the same transverse planes as in Fig. 4. Before breakdown, the leading-edge vortex core presents strong negative vorticity levels (Figs. 5a and 5b). Higher levels are observed on the axis upstream of the breakdown on model 2. Downstream of the breakdown (Figs. 5c and 5d), vorticity levels are reduced due to both radial and axial flow decelerations. Finally, other highly rotational zones are discernible in the flowfield both upstream and downstream of the breakdown location. These comprise the shear layer separating from the leading edge and a secondary vortex that is counter-rotating, compared with the primary vortex [16]. Axial vorticity levels are high and these structures do not seem to be altered by the primary vortex breakdown. The meshes of the transverse planes over model 2 do not cover the flowfield sufficiently close to the leeward side to allow the observation of these vortical zones.

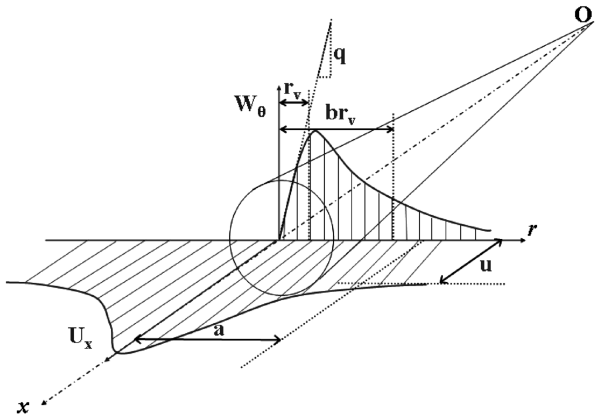

Fig. 6 Nondimensional velocity distribution examples with description of the nondimensional parameters.

IV. Inviscid Linear Temporal Stability of the Delta Wing Vortices

A. Cylindrical Basic Flow Model

We interpolate the experimental values by considering cylindrical coordinates x, r, and θ centered on the vortex centerline, where the x axis corresponds to the vortex axis and the r axis corresponds to its radius (Fig. 2). In the cylindrical frame, the velocity components are U_x, V_r, and W_θ and are assumed to depend only on r, which suggests that variations of the flow are weak in the longitudinal direction. Away from the breakdown location, this hypothesis is acceptable. However, the columnar assumption is clearly violated at the breakdown location. Accounting for axial flow variations would require a spatial stability analysis approach (see [24] and references therein).

We assume a positive azimuthal velocity, corresponding to starboard primary vortices rotating counterclockwise in the r–θ plane. The basic flow model, in terms of dimensional variables indicated by a superscript star, is considered in the following form:

$$U_x^\star(r^\star) = U_{0,x} + Ae^{-(r^\star/A_1)^2} + Be^{-(r^\star/A_2)^3}, \qquad V_r^\star(r^\star) = 0,$$
$$W_\theta^\star(r^\star) = \frac{\Omega_0 r^\star}{[1+(r^\star/B_1)^2]^{(\frac{1+N}{2})} \times [1+(r^\star/B_2)^2]^{(\frac{1-N}{2})}} \tag{1}$$

The expression for the axial velocity is the sum of a Gaussian distribution and a term introduced to fit axial velocity profiles downstream of the vortex breakdown, for which the extremum is shifted away from the x axis (see Figs. 4c and 4d). For $B = 0$, we retrieve the Gaussian formulation, $U_{0,x}$ is the freestream velocity component along the x axis, $A + B = U_x^\star(0) - U_{x,0} = \Delta U$ is the centerline axial velocity defect, A_1 denotes the jet core size, and A_2 is a measure of the radius of maximum axial velocity when it is distinct from the x axis.

The expression for the azimuthal velocity is derived from a model used to study the properties of the short-wave cooperative instabilities of aircraft wakes [25]. This law corresponds to the superposition of a solid body rotation on the axis, a potential zone away from the axis, and an intermediate rotational zone. B_1 is a size of the solid body rotation region and B_2 is the external radius above which a potential law holds. N is the exponent of the power law representative of the intermediate rotational zone (i.e., $W_\theta^\star(r^\star) \sim \Omega_0 B_1 (r^\star/B_1)^{-N}$ and $B_1 < r^\star < B_2$).

Using the centerline axial velocity defect ΔU and the jet core size A_1 as velocity and length scales, the nondimensional expressions (without a superscript star) for the basic flow become

$$U_x(r) = u + \delta e^{-r^2} + (1-\delta)e^{-(r/a)^3}, \qquad V_r(r) = 0,$$
$$W_\theta(r) = \frac{qr}{[1+(r/r_v)^2]^{(\frac{1+N}{2})} \times [1+(r/br_v)^2]^{(\frac{1-N}{2})}} \tag{2}$$

where $u = U_{0,x}/\Delta U$ denotes the external flow parameter that compares the freestream velocity with the axial velocity defect (Fig. 6), $u > 0$ refers to a coflowing jet, $u < -1$ refers to a coflowing wake, $-1 < u < 0$ refers to a counterflowing jet or wake, the parameter δ quantifies the deviation of the axial velocity distribution from a Gaussian distribution (if $\delta = 1$, the Gaussian formulation is recovered), $a = A_2/A_1$ is the jet radii ratio, the swirl parameter $q = \Omega_0 A_1/\Delta U$ measures the intensity of rotation compared with that of advection, $r_v = B_1/A_1$ is the axial to azimuthal length scales ratio, and $b = B_2/B_1$ denotes the external and internal vortex core scales ratio (a value of b close to unity indicates that the vorticity is concentrated in the vortex core).

Table 1 summarizes the parameter values obtained by fitting experimental axial and azimuthal velocity profiles for each plane by means of a least-squares algorithm. Reynolds numbers $Re = \Delta U A_1/\nu$, based on velocity and length scales, are also given. Measurement planes are perpendicular to the root chord, and velocity fields are expressed in Cartesian coordinates. The vortex x axis is at an angle β_1 to the leeward-side plane and at an angle β_2 to the

Table 1 Nondimensional parameter values obtained by fitting experimental data in each measurement plane with model (2); corresponding Reynolds numbers and standard deviations (bold type) of the model vs the experiments (in percent of the freestream velocity); upstream and downstream planes are with respect to the vortex breakdown location

	Model 1, $\alpha = 18$ deg				Model 2, $\alpha = 30$ deg			
	Upstream		Downstream		Upstream		Downstream	
X/c	0.22	0.36	0.47	0.51	0.32	0.45	0.53	0.84
u	1.0	0.9	2.8	−1.1	0.5	0.4	−0.7	−1.4
δ	0.95	0.95	−0.71	1.43	0.68	0.49	2.02	0.22
a	0.24	0.25	5.13	2.94	4.51	3.55	5.98	2.16
q	3.4	3.7	2.2	−0.5	2.9	4.8	−1.1	−0.5
r_v	0.48	0.21	1.64	0.41	0.41	0.14	1.86	0.66
b	20.5	5.96	7.10	5.13	60.0	24.4	26.9	2.09
N	0.14	−0.45	−0.08	−1.57	0.39	−0.08	0.42	1.94
$10^{-4} \times Re$	3.0	5.8	0.5	3.2	5.7	4.4	1.4	1.8
σ_{U_x} [%]	**0.52**	**0.53**	**0.77**	**0.52**	**2.82**	**3.95**	**6.46**	**0.91**
σ_{W_θ} [%]	**0.75**	**1.04**	**0.26**	**0.66**	**6.85**	**3.05**	**6.48**	**2.07**

symmetry plane of the model (Fig. 2). Therefore, we must apply two rotations on the Cartesian frame to center the Cartesian X axis on the vortex x axis and express the new Cartesian coordinates into cylindrical coordinates. The same transformation is then applied to the velocity components; β_1 and β_2 are chosen so that the points of maximum axial velocity and axial vorticity match. This point is then defined as the center of the vortex. Finally, average velocities along circles of radius r are retained to obtain axisymmetric fields $[U_x(r), 0, W_\theta(r)]$. Standard deviations of theoretical laws from experimental data are given in percentage of the freestream velocity U_0.

The general trends underlined in Sec. III are retrieved. The axial velocity distribution evolves from a coflowing jetlike profile upstream to a wakelike profile downstream of the breakdown, with a coflow over model 1 and with a counterflow over model 2. Downstream, the maximum velocity is located at a finite distance from the axis and separates an inner region of negative azimuthal vorticity from an outer region of positive vorticity.

In accordance with the vorticity distributions of Fig. 5, the azimuthal velocity profiles exhibit high levels of solid body rotation close to the centerline upstream of the breakdown, with stronger values for model 2 than for model 1. This difference between models 1 and 2 is due to the changes in sweep angle φ and wing incidence α. Following the Kutta–Joukowski theorem with the assumption of a two-dimensional potential flow independent of X, the circulation of the vortex at a fixed station X is proportional to $\Gamma_0(X) \sim U_0(\sin\alpha)s(X)$, where $U_0 \sin\alpha$ is the freestream velocity component in the transverse Y–Z plane, and $s(X) = X/\tan\varphi$ denotes the local semispan of the delta wing. Then the rotation rate of the vortex on its axis may be evaluated by $\Omega_0 \sim \Gamma_0/r_e^2$, where r_e is a measure of the radius of a Rankine vortex with the same circulation (i.e., $\Omega_x(r) = \Omega_0$ if $r < r_e$ and $\Omega_x(r) = 0$ if $r > r_e$). With the assumption of a conical delta wing flowfield, we have $r_e \sim s(X)$. From these considerations, it follows directly that

$$\frac{\Omega_0 c}{U_0} \sim \frac{\sin\alpha \tan\varphi}{X/c} \tag{3}$$

Thus, for an equivalent nondimensional abscissa X/c, the nondimensional vorticity $\Omega_x c/U_0$ around the axis is greater for model 2 than for model 1. Moreover, $\Omega_x c/U_0$ is a decreasing function of X/c. Downstream, the rotation rate and swirl level are lower and the maximum of velocity is pushed away from the axis, indicating a widening of the vortex core.

B. Stability of Vortices: A Short Review

The inviscid stability analysis consists of linearizing the Euler equations around a basic flow with superimposed infinitesimal perturbations. Using cylindrical coordinates x, r, and θ, we focus our attention on inviscid, incompressible, and permanent columnar vortices of the form $[U_x(r), 0, W_\theta(r)]$. The Reynolds numbers of the vortex flows are high (see Table 1) and allow us to neglect viscous effects. Taking advantage of axisymmetry and invariance under x and t translations, one can decompose these perturbations into normal modes proportional to $\exp\{i(kx + m\theta - \omega t)\}$. Solving the resulting equations with boundary conditions leads to a dispersion relation invoking pulsation ω, axial k, and azimuthal m wave numbers. Temporal analysis assumes k to be real, and for any given pair of k and m, solutions are the complex eigenvalues $\omega = \omega_r + i\omega_i$, where ω_i and ω_r are the temporal growth rate and frequency of the perturbation. Stability of the basic state is characterized by the sign of the maximum temporal growth rate $\omega_{i,\max}$. The basic state is either linearly unstable if $\omega_{i,\max} > 0$ or linearly stable if $\omega_{i,\max} \le 0$. If $\omega_{i,\max} = 0$, then the basic state is said to be neutrally stable. Development into normal modes induces invariance of the perturbations through the transformation of k, m, and ω to $-k$, $-m$, and $-\bar{\omega}$ and allows us to restrict the study to positive values of k ($\bar{\omega}$ refers to the complex conjugate of ω).

1. Temporal Stability Analysis

As mentioned in the Introduction, LS developed a sufficient condition for the instability of a columnar vortex to helical perturbations valid for $|m| \gg 1$:

$$\exists r| \qquad W_\theta \Omega'[\Gamma'\Omega' + (U_x')^2] < 0 \tag{4}$$

where primes denote derivatives with respect to r, and $\Gamma = rW_\theta$ and $\Omega = W_\theta/r$ are the angular momentum per unit mass of a fluid element and the angular velocity of the basic flow, respectively. If $U_x' \equiv 0$, one recovers Rayleigh's criterion for centrifugal instability: a two-dimensional vortex is stable to axisymmetric disturbances if, and only if, its circulation is a strictly increasing function of the radius r. This asymptotic analysis demonstrates that negative modes $m < 0$ are destabilized, with a maximum growth rate that increases with $|m|$ and tends to a limit such as $m \to -\infty$. LS were able to derive an analytical expression for the asymptotic growth rate. Moreover, they showed that unstable modes are concentrated in the neighborhood of a critical radius r_0 and they therefore called them *ring modes*. Their results account for the theoretical work of Ludwieg [26], which indicates that the most unstable waves in a narrow annular gap are negative, with

$$-\frac{k}{m} = \frac{\Omega'(r_0)}{U_x'(r_0)} \tag{5}$$

2. Critical-State Theory

Benjamin [17] proposed a theory to explain the vortex breakdown occurrence by relating this phenomenon to the existence of stationary axisymmetric waves in the vortex core. This theory is based on neutrally stable inertial waves of infinite extent or Kelvin waves. According to Benjamin, a vortex breakdown is the result of a transition from a supercritical flow supporting only downstream traveling waves to a subcritical state supporting both upstream and downstream propagating waves. Benjamin derived a criterion based on the minimum phase velocity of the axisymmetric Kelvin waves: $c_- > 0$ indicates a supercritical flow and $c_- < 0$ indicates a subcritical flow.

From this theory, it is possible to derive an analytical criterion that determines the criticality of a vortex model. The case of a solid body rotation and constant advection in a pipe ($U_x^\star(r^\star) = U_x^\star(0)$ and $W_\theta^\star(r^\star) = \Omega_0 r^\star$ for $r^\star \in [0, R_c]$) is treated in [27]. The minimum phase speed of the axisymmetric inertial waves is obtained in the limit $k = 0$ and reaches $c_- = -2\Omega_0 R_c/j_{1,1} + U_x^\star(0)$, where $j_{1,1}$ is the first zero of the Bessel function of first kind J_1. The criticality of this model is hence a function of a swirl parameter q_0; the flow is supercritical when

$$q_0 = \frac{\Omega_0 R_c}{U_x^\star(0)} < \frac{j_{1,1}}{2} \tag{6}$$

and subcritical when $q_0 > j_{1,1}/2$. This model will be applied to our velocity measurements (Sec. IV.E).

C. Numerical Method

Numerical treatment is performed by using a spectral method implemented by Fabre and Jacquin [28]. Functions are developed using Chebyshev series expansions and evaluated at collocation points for which the distribution is controlled. This method was successfully applied to the temporal stability analysis of trailing-line-vortex models [28].

For a helical mode $m \neq 0$, the sense of winding of the perturbation is compared with that of the basic flow. The trajectories of the basic flow fulfill $\mathrm{d}\theta/\mathrm{d}x = W_\theta/rU_x$, and so they roll up in a direct sense, when traveling in the x direction, when this quantity is positive. The surfaces of constant phase $kx + m\theta - \omega_r t = \text{const}$ follow spirals with an helix angle of $\mathrm{d}\theta/\mathrm{d}x = -k/m$. Thus, the perturbation is corotating (respectively, counter-rotating) if the senses of winding of the basic flow and of the helix are identical (respectively, opposite).

Table 2 LS asymptotic criterion results for nondimensional maximum growth rate $\omega_{i,\infty}/\Omega_0$ and critical radius r_0/r_c; criticality of leading-edge vortices for minimum phase velocity c_- (numerical results) and swirl number $q_0(X/c)$ compared with the critical swirl $j_{1,1}/2$ of the pipe flow model (6); upstream and downstream planes are with respect to the vortex breakdown location.

	Model 1, $\alpha = 18$ deg				Model 2, $\alpha = 30$ deg			
	Upstream		Downstream		Upstream		Downstream	
X/c	0.22	0.36	0.47	0.51	0.32	0.45	0.53	0.84
$\omega_{i,\infty}/\Omega_0$	——	——	——	0.62	——	0.02	0.59/0.05	0.46
r_0/r_c	——	——	——	0.49	——	3.59	0.36/2.15	0.38
$c_-/\Omega_0 r_c$	0.16	0.11	0.02	−0.43	0.10	0.05	−0.34	0.20
$2q_0/j_{1,1}$	0.80	0.98	1.55	12.8	0.69	0.72	4.82	3.04

D. Stability Results

Table 2 displays results of the LS criterion (4) applied to our velocity measurements and indicates a centrifugal instability mechanism in planes $X/c = 0.51$ (model 1) and $X/c = 0.84$, 0.45, and 0.53 (model 2). Values are nondimensionalized by Ω_0 and by the radius of maximum azimuthal velocity, r_c. Note that there is a second local positive maximum for the growth rate in the plane $X/c = 0.53$. This maximum is lower than the first and occurs at a larger radius.

Figure 7 presents the growth rates ω_i and frequencies ω_r as functions of k for each destabilized mode over model 1. Numerical results are consistent with LS asymptotic theory: only the last plane $X/c = 0.51$ exhibits destabilized temporal branches, the other planes are neutrally stable to any infinitesimal perturbations and do not verify the LS criterion. Only the 15 first inviscid modes are drawn, but we can expect that an infinite number of counter-rotating helical perturbations exist, for which the largest growth rate tends to an asymptotic limit close to the prediction of LS as $m \to \infty$ (see Fig. 7a). The mode $m = 2$ possesses an overall maximum growth rate for an axial wave number $k_{\max} r_c = 1.19$; the largest amplification rate of each azimuthal mode decreases until $m = 5$ and then increases toward the asymptotic limit. All frequencies are positive, indicating positive azimuthal phase velocities ω_r/m that correspond to corotating perturbations in time with respect to the basic flow. Note that in the limit of two-dimensional waves, each instability becomes neutral ($\lim_{kr_c \to 0} \omega_i/\Omega_0 = 0$) with frequency that verifies $\lim_{kr_c \to 0} \omega_r/\Omega_0 = m$, corresponding to the intrinsic period of oscillation of a column of fluid [27]. Figure 8d displays an example of the radial structure of the modes in which the vorticity is concentrated in the vicinity of a particular radius located in the vortex core, as predicted by the LS theory (Table 2). Finally, the axisymmetric mode $m = 0$ is found to be stable.

Stability results for model 2 are similar (results not shown here) and confirm the asymptotic predictions of LS. The basic flow is linearly unstable to helical perturbations in the three last planes. As $|m| \to \infty$, their maximum amplification rates tend to the asymptotic value of LS. However, these modes are qualitatively different from their counterparts observed over model 1. First, the plane $X/c = 0.47$ is located upstream of the breakdown, whereas other upstream planes are stable. These perturbations are weakly amplified compared with the others. We emphasize that if swirl exceeds a certain level in the vortex model (2), the LS criterion is not verified and the flow is stabilized. Strong rotation levels, compared with advection, that generally occur upstream of the vortex breakdown could stabilize the flow. This feature is similar to the $q < \sqrt{2}$ stability condition for a q vortex, where $U_x(r) = u + \exp(-r^2)$ and $W_\theta(r) = q[1 - \exp(-r^2)]/r$ (see [11]). Second, co- and counter-rotating helical modes are amplified in the plane $X/c = 0.53$, the corotating modes being less amplified than the counter-rotating modes by approximately one decade. Finally, in the planes $X/c = 0.45$ and 0.53, some particular modes have zero phase velocity and are stationary in the delta wing frame.

Further comparisons could be done with the asymptotic theory of LS by exploring some characteristics of the instabilities as a function of m. The eigenfunctions of each mode are concentrated in the vicinity of a radius $r(m)$; Fig. 8 shows the evolutions of this radius, of the helix angle $\beta = -k/m$, and of the maximum amplification rate $\omega_{i,\max}$ with $|m|$. Values are nondimensionalized by the theoretical values of LS. In each plane, the classes of perturbations exhibit trends predicted by the LS theory. The maximum amplification rate is an increasing function of $|m|$ and is bounded from above by $\omega_{i,\infty}$. The plane $X/c = 0.53$ from the model 2 flowfield presents two families of such ring modes. The most amplified family is associated with a lower critical radius in a region of positive radial gradient of axial velocity $U_x' > 0$ and owns a negative helix angle $\beta < 0$, whereas the other family develops in an outside region in which $U_x' < 0$ and $\beta > 0$. In both cases, instabilities fulfill condition (5).

To conclude this inviscid linear temporal stability analysis of the delta wing vortex flows, we retain that

1) Upstream of the vortex breakdown, leading-edge vortices are either linearly stable or weakly unstable to infinitesimal perturbations. Downstream, ring modes are strongly amplified via a centrifugal instability mechanism.

2) Some particular modes over model 2 are stationary in the planes $X/c = 0.45$ and 0.53.

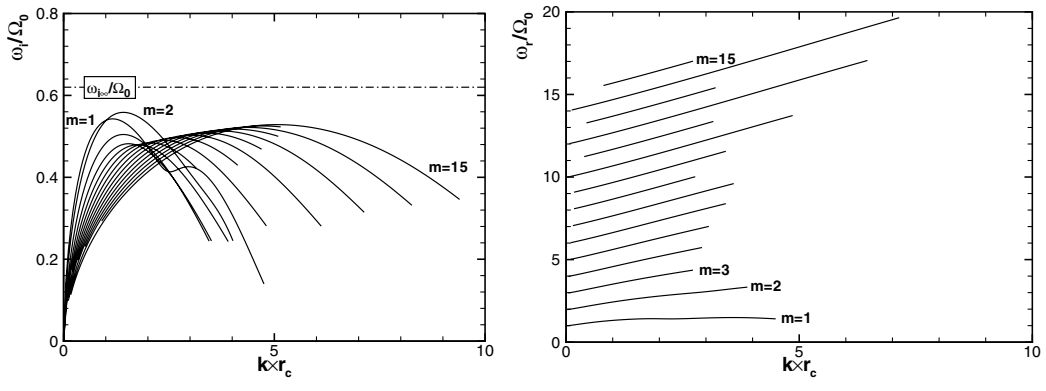

Fig. 7 Model 1 instability characteristics: a) nondimensional amplification rates $\omega_i(m,k)/\Omega_0$ and b) pulsations $\omega_r(m,k)/\Omega_0$ as functions of the nondimensional wave number kr_c for the 15 first temporal branches (plane $X/c = 0.51$); in Fig. 7a, the horizontal dash-dots correspond to the maximum growth rate from the LS asymptotic prediction $\omega_{i,\infty}/\Omega_0$.

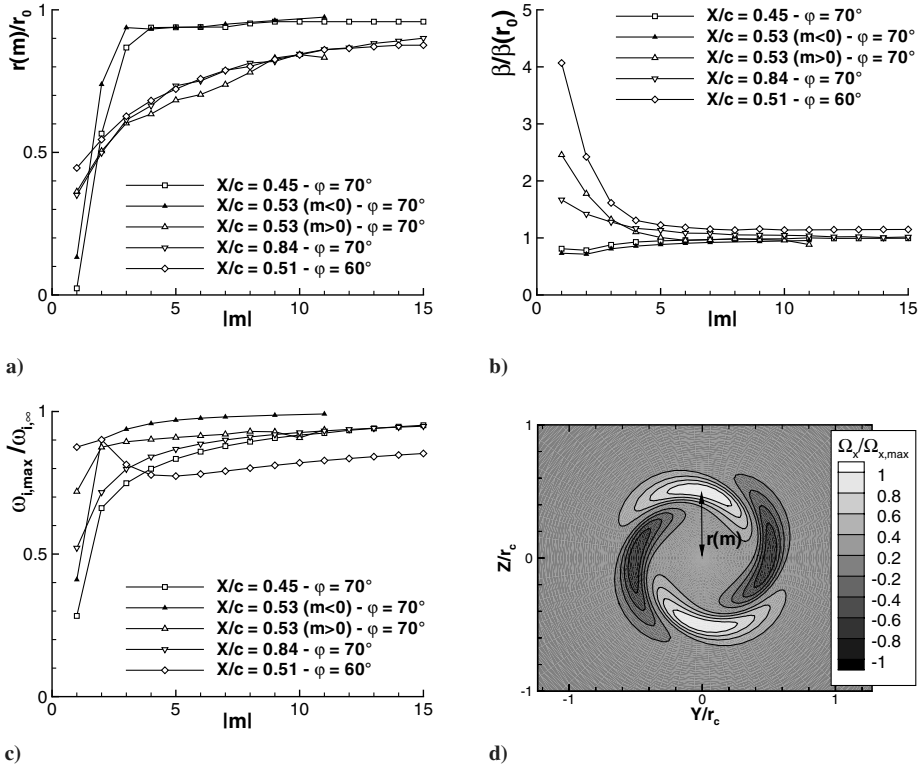

Fig. 8 Instability characteristics: a) eigenfunction radii, b) helix angles, c) maximum amplification rates as functions of $|m|$, and d) axial vorticity contours of the most amplified eigenfunction ($m = 2, k_{\max} r_c = 1.19$, model 1) in which levels have been arbitrarily dimensionalized; the radius $r(m)$ is evaluated from inspection of the transverse distributions of each eigenfunction, as represented in Fig. 8d; values are nondimensionalized with asymptotic values of LS [$\beta(r_0)$ is obtained from the right-hand side of Eq. (5) and r_0 denotes the radius from LS theory (see Table 2)].

3) The characteristics of each instability could be well predicted by the LS theory. Likewise, their amplification rates are of the same order as the vortex rotation rate (see Table 2), which could be estimated via Eq. (3) and experimental conditions.

E. Kelvin Mode Dynamics: Comparison with the Critical-State Theory

We now focus our attention on axisymmetric neutral waves $m = 0$ and their contributions to vortex breakdown according to Benjamin's criterion (6). In the present vortex flows, such waves are neutral ($\omega_i = 0$) and are propagating inertial waves. Benjamin's criterion is based on the sign of infinitely long and axisymmetric Kelvin waves c_-, for which the values are given in Table 2. Phase velocities are positive and the flow is supercritical upstream of and in the planes close to the vortex breakdown. Downstream of the breakdown, c_- is always negative and some Kelvin waves propagate upstream, therefore the flow is subcritical. The minimum phase velocity decreases from upstream to downstream of the breakdown in accordance with a decreasing effect of Doppler shift associated with a decreasing advection amplitude compared with that of rotation. According to the critical-state concept and to our experiments, delta wing vortices are supercritical upstream of the vortex breakdown and subcritical downstream of it.

The analytical criterion for critical vortex flows (6) is based on the assumption that the vortex core behaves like a waveguide for the infinitely long Kelvin waves. Comparisons between experimental data and this model are shown in Table 2. The best-fitting parameters provide the value of the swirl number $q_0 = qr_c/(1 + u)$ in each plane and thus give a prediction of the flow criticality. The pipe flow model agrees with the occurrence of vortex breakdown in our flows. A deeper comparison was done by considering the effect of the vortex model parameters. We focus on the dynamic behavior of inertial waves. A leading-term analysis of the linearized Euler equations around the vortex axis shows that the more relevant parameters of the vortex model (2) are the swirl q, the external flow parameter u, and the parameter δ, because only these parameters

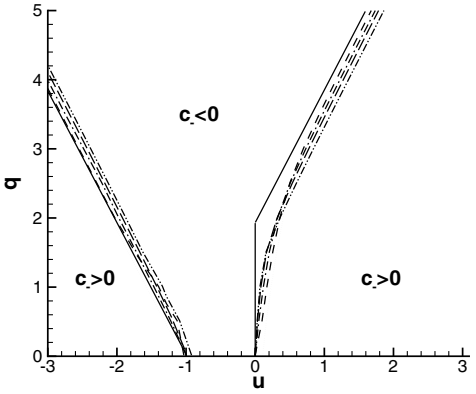

Fig. 9 Criticality in the q–u parameter plane for model (2) (dot: $\delta = -2$, dash: $\delta = -1$, dash-dot: $\delta = 0$, long dash: $\delta = 1$, and dash-dot-dot: $\delta = 2$) and model (6) (solid lines).

account for the velocity field in the vortex core. For simplification, all results presented here are obtained with $a = b = 1$. We evaluate the sign of the minimum phase speed c_- of the axisymmetric Kelvin waves in the limit $kr_c = 0$. Such waves are neutral; critical layers may therefore appear at a radius r when $\omega_r = kU_x(r) + m\Omega(r)$ and create numerical problems. Practically, these values are reached close to $q = 0$ and are not treated in the present study.

Figure 9 displays criticality of the vortex flow model (2) in the q–u parameter space for several values of the parameter δ. Lines separate supercritical from subcritical states. We only consider positive swirl values without loss of generality, because axisymmetric waves behave independently of the rotation sense of the vortex. These results are qualitatively similar to the corresponding study of the q vortex model (see Fig. 8 in [2]). The parameter δ does not have an important effect on the criticality, because it does not govern either the length scale or the velocity scale. As expected, an increase in

swirl q leads to the subcritical state by decreasing the minimum phase speed c_-, whereas an increase in the absolute value of the external parameter $|u|$ furthers supercritical conditions by advecting waves downstream of the flow. Furthermore, for either coflowing jets $u > 0$ or coflowing wakes $u < -1$ and for sufficiently large swirl values, the boundary between critical states is close to the dispersion relation of the pipe flow model (6). The wavelengths of such waves are infinitely large compared with the transverse length scale, and the vortex core acts like a waveguide. Nevertheless, in the case of strong coflowing jets (i.e., little swirl values), the critical conditions diverge. The Doppler effect becomes so strong that the minimum wave phase speed depends only on u. This effect reduces for coflowing wakes. Finally, note that reversal flows corresponding to counterflowing wakes or jets $-1 < u < 0$ are always subcritical.

V. Conclusions

The leading-edge vortex development over two delta wings with different geometries is examined using LDV. From experimental measurements, an analytical model is formulated that fits the mean velocity fields upstream and downstream of the vortex breakdown location. A linear temporal and inviscid stability study provides detailed characteristics of infinitesimal perturbation evolutions and of neutrally stable inertial wave dynamics.

On one hand, this analysis highlights the temporal stability of such flows, with the identification of physical mechanisms leading to instability as the main purpose. Upstream of the vortex breakdown, the swirl levels are strong and axial velocities have jetlike profiles with distributions close to Gaussian. The LS condition taking axial velocity into consideration is verified only in one plane $X/c = 0.45$ upstream of the vortex breakdown over model 2. In the same manner, the numerical simulations show that disturbances are either damped or weakly amplified.

In the downstream planes, the basic flow exhibits lower swirl levels. Moreover, the extremum of axial velocity is located at a radius distinct from the vortex axis and is associated with an inner region of positive azimuthal vorticity surrounded by a region of negative vorticity. The temporal instability analysis reveals that a large range of negative helical ring modes is amplified downstream. Their characteristics agree with the asymptotic predictions of LS and could be roughly estimated by Eq. (3) and by assuming that $\omega_{i,\infty}/\Omega_0 = O(1)$. Finally, in some planes over model 2 ($X/c = 0.47$ and 0.53), stationary corotating helical modes are destabilized in an external region, in which $U'_x < 0$ ($\beta > 0$), and agree with LS analysis too. These modes are slightly amplified and low-dispersive during their travel above the delta wing. Nevertheless, these perturbations are not observed in our experiments. Further comparisons should be done with the steady substructures developing in the shear layer of delta wing flows [29] and observed at a lower incidence $\alpha = 27$ deg over model 2 [30].

On the other hand, we use the critical-state theory of Benjamin [17], on the basis of neutrally stable inertial waves of infinite extent, to evaluate the basic flow parameter effects on its criticality. We first verify the criterion in the case of our experimental results. Upstream of the breakdown, phase velocities of nondispersive Kelvin waves are positive and travel only downstream in the vortex; the basic flow is supercritical. Downstream, the minimum phase velocities reach negative values. The leading-edge vortices are subcritical and undergo a broken state. Moreover, the criticality of delta wing flows could be easily estimated by means of model (6), based on the mean flow characteristics. A local analysis of the spatiotemporal development of disturbances would bring information on the absolute/convective transition properties of the basic flow and their link with the vortex breakdown mechanism .

By varying the parameter values of model (2), we estimate the effect of the basic flow distribution on its criticality. As expected, an increasing swirl value q promotes the subcritical state by decreasing the minimum phase velocity. A raising absolute value of the external parameter $|u|$ increases the advection of Kelvin waves and thus furthers the supercritical state by a Doppler effect. Surprisingly, the parameter δ does not affect the criticality, whereas it strongly modifies the local stability properties. We recall that δ is away from unity when the maximum of mean axial velocity is distinct from the vortex axis as a consequence of the presence of the mixing layer and secondary vortices above the wing. The core flow is mainly governed by its transverse length scale, which is a measure of the solid body rotation zone and is independent of δ. The vortex core behaves like a waveguide for the Kelvin waves of infinite extent.

These results account for the stability control of vortical delta wing flowfields by manipulating flow magnitudes, the swirl number q, the external flow parameter u, and the vortex core radius.

Acknowledgment

The authors warmly acknowledge David Fabre who provided numerical tools and fruitful suggestions.

References

[1] Hall, M. G., "A Theory for the Core of a Leading-Edge Vortex," *Journal of Fluid Mechanics*, Vol. 11, 1961, pp. 209–228.
[2] Leibovich, S., "Vortex Stability and Breakdown: Survey and Extension," *AIAA Journal*, Vol. 22, No. 9, 1984, pp. 1192–1206.
[3] Rusak, Z., and Wang, S., "Review of Theoretical Approaches to the Vortex Breakdown Phenomenon," AIAA Paper 96-2126, 1996.
[4] Mitchell, A. M., and Délery, J., "Research into Vortex Breakdown Control," *Progress in Aerospace Sciences*, Vol. 37, No. 4, 2001, pp. 385–418.
[5] Renac, F., "Contrôle Expérimental de l'écoulement Tourbillonnaire sur une aile delta," Ph.D. Thesis, Univ. Paris VI, Paris, 2004.
[6] Mitchell, A. M., "Caractérisation et Contrôle de L'Éclatement Tourbillonnaire sur une aile Delta aux Hautes Incidences," Ph.D. Thesis, Univ. Paris VI, Paris, 2000.
[7] Reau, N., and Tumin, A., "Harmonic Perturbations in Turbulent Wakes," *AIAA Journal*, Vol. 40, No. 3, 2002, pp. 526–530.
[8] Jacquin, L., and Pantano, C., "On the Persistence of Trailing Vortices," *Journal of Fluid Mechanics*, Vol. 471, Nov. 2002, pp. 159–168.
[9] Lesen, M., Singh, P. J., and Paillet, F., "The Stability of a Trailing Line Vortex, Part 1: Inviscid Theory," *Journal of Fluid Mechanics*, Vol. 63, 1974, pp. 753–763.
[10] Batchelor, G. K., "Axial Flow in Trailing Line Vortices," *Journal of Fluid Mechanics*, Vol. 20, 1964, pp. 645–658.
[11] Leibovich, S., and Stewartson, K., "A Sufficient Condition for the Instability of Columnar Vortices," *Journal of Fluid Mechanics*, Vol. 126, 1983, pp. 335–356.
[12] Garg, A. K., and Leibovich, S., "Spectral Characteristics of Vortex Breakdown Flowfields," *Physics of Fluids*, Vol. 22, Nov. 1979, pp. 2053–2064.
[13] Gursul, I., "Unsteady Flow Phenomena over Delta Wings at High Angle of Attack," *AIAA Journal*, Vol. 32, No. 2, 1994, pp. 225–231.
[14] Lambourne, N. C., and Bryer, D. W., "The Bursting of Leading Edge Vortices—Some Observations and Discussion of the Phenomenon," Aeronautical Research Council, Reports and Memoranda No. 3282, London, 1961.
[15] Singh, P. I., and Uberoi, M. S., "Experiments on Vortex Stability," *Physics of Fluids*, Vol. 19, No. 12, Dec. 1976, pp. 1858–1863.
[16] Gordnier, R. E., and Visbal, M. R., "Unsteady Vortex Structure over a Delta Wing," *Journal of Aircraft*, Vol. 31, No. 1, 1994, pp. 243–248.
[17] Benjamin, T. B., "Theory of the Vortex Breakdown Phenomenon," *Journal of Fluid Mechanics*, Vol. 14, 1962, pp. 593–629.
[18] Tsai, C.-Y., and Widnall, S. E., "Examination of Group-Velocity Criterion for Breakdown of Vortex Flow in a Divergent Duct," *Physics of Fluids*, Vol. 23, May 1980, pp. 864–870.
[19] Escudier, M. P., Bornstein, J., and Maxworthy, T., "The Dynamics of Confined Vortices," *Proceedings of the Royal Society of London A*, Vol. 382, No. 1783, 1982, pp. 335–360.
[20] Ruith, M. R., Chen, P., Meiburg, E., and Maxworthy, T., "Three-Dimensional Vortex Breakdown in Swirling Jets and Wakes: Direct Numerical Simulation," *Journal of Fluid Mechanics*, Vol. 486, July 2003, pp. 331–378.
[21] Micheli, F., Losfeld, G., and Girardot, L., "Incertitudes de Mesure sur la Variance de la Troisième Composante," 8ème Congrès Francophone de Vélocimétrie Laser, Orsay, France, Laboratoire d'Informatique pour la Mécanique et les Sciences de l'Ingénieur, Orsay, France, and Centre National de la Recherche Scientifique, Orsay, France, 2002.
[22] Rockwell, D., "Three-Dimensional Flow Structure on Delta Wings at High Angle-Of-Attack: Experimental Concepts and Issues," AIAA Paper 93-0550, 1993.

[23] Towfighi, J., and Rockwell, D., "Instantaneous Structure of Vortex Breakdown on a Delta Wing via Particle Image Velocimetry," *AIAA Journal*, Vol. 31, No. 6, 1993, pp. 1160–1162.
[24] Herrada, M. A., Pérez-Saborid, M., and Barrero, A., "Nonparallel Local Spatial Stability Analysis of Pipe Entrance Swirling Flows," *Physics of Fluids*, Vol. 16, No. 7, 2004, pp. 2147–2153.
[25] Fabre, D., and Jacquin, L., "Short-Wave Cooperative Instabilities in Representative Aircraft Vortices," *Physics of Fluids*, Vol. 16, No. 5, 2004, pp. 1366–1378.
[26] Ludwieg, H., "Stabilität der Strömung in Einem Zylindrischen Ringraum," *Zeitschrift für Flugwissenschaften*, Vol. 8, No. 5, 1960, pp. 135–140.
[27] Chandrasekhar, S., *Hydrodynamic and Hydromagnetic Stability*, Clarendon, Oxford, 1961.
[28] Fabre, D., and Jacquin, L., "Viscous Instabilities in Trailing Vortices at Large Swirl Numbers," *Journal of Fluid Mechanics*, Vol. 500, Feb. 2004, pp. 239–262.
[29] Visbal, M., and Gordnier, R., "On the Structure of the Shear Layer Emanating from a Swept Leading Edge at Angle of Attack," AIAA Paper 2003-4016, 2003.
[30] Mitchell, A. M., and Molton, P., "Vortical Substructures in the Shear Layers Forming Leading-Edge Vortices," *AIAA Journal*, Vol. 40, No. 8, 2002, pp. 1689–1692.
[31] Gallaire, F., and Chomaz, J.-M., "Mode Selection in Swirling Jet Experiments: A Linear Stability Analysis," *Journal of Fluid Mechanics*, Vol. 494, Nov. 2003, pp. 223–253.

A. Tumin
Associate Editor